New Journal and we have not received input yet 32 (2022) 101237

Contents lists available at ScienceDirect

Thermal Science and Engineering Progress

journal homepage: www.elsevier.com/locate/tsep

An internal flow and heat transfer inside a solid rocket motor combustion chamber; A Lie symmetry approach

Karabo Modise, Gabriel Magalakwe *

School of Mathematical and Statistical Sciences, North-West University, Potchefstroom Campus, Private Bag X6001, Potchefstroom 2520, Republic of South Africa

ARTICLE INFO

Keywords:
Lie symmetry approach
Propellant flow
Heat distribution
Double-perturbation technique
Porous surface
Solid rocket operation

ABSTRACT

The validity of Solid Rocket Motor (SRM) stability calculations critically depends on the sufficiently detailed and physically correct representation of propellant velocity flow-field, which leads to well behaved flow. A theoretical analysis of propellant flow and heat distribution is presented to study the thermal effects on propellant velocity flow-field to understand rocket stability dynamics better. Analysis based on Lie symmetry and perturbation technique is used to construct semi-analytical propellant flow and heat distribution solutions. Effects of various non-dimensional parameters arising from the Solid Rocket Motor design are graphically represented, analysed and parameter values leading to unstable and stable propellant flow are quantified. The study mainly gives an insight of thermal parameters affects rocket momentum. Among other findings, the study found that for Prandtl number values $P_r > 0.1$ while sucking propellant out of the combustion chamber leads to instabilities on the propellant velocity flow field. In contrast, same P_r values lead to stable operation during injection. Also, the results show that for Grashof number values $G_r > 0.1$ while injecting propellant into the combustion leads to unstable propellant velocity field but stable flow velocity during suction. The obtained temperature profiles agree with the experimental and theoretical results from the literature.

1. Introduction

In the past and recently, the topic of fluid flow, driven by injection through porous pipes, has received significant attention due to the wide industrial importance and technical applications covered by this topic. Such industrial importance and technical applications are boundary layer control, surface transpiration and modelling of Solid Rocket Motor (SRM) propellant grain. Focusing the attention of the subject at hand to modelling SRM propellant grain, stability prediction methods play a crucial role in the steady state operation of SRM. Culick in [1,2] set the groundwork for predicting the steady state operation of SRM by adopting three assumptions. Firstly, perturbation representation of internal velocity can be used for small propellant velocity amplitude. Secondly, a simple boundary condition imposed at the chamber surface can represent all surface reactions. Lastly, all physical parameters that lead to rotational flow effects have negligible influence on combustion stability, as mentioned in [3]. The studies discussed above undertaken by Culick indicate the advantage of semi-analytical techniques such as the perturbation method, which is the technique that linearises the governing equations by using the parameters that affect the system flow and heat distribution as perturbation quantities.

From various unstable motions observed in SRM chambers, currently the most challenging are those involving oscillatory motions parallel to the flow axis. SRM instabilities are due to velocity fluctuations parallel to the combustion chamber surface. This phenomenon is known as velocity coupling, and these instabilities can be understood by studying the axial velocity as in [4]. Motivated by the studies mentioned above, theoretical injection-driven flow studies have been initiated to further understand these instabilities in an SRM using porous pipes. The instabilities of such aeroacoustic solutions of porous pipe flow driven by fluid injection, which later served as a reasonable approximation for analysis of propellant inside a combustion chamber, were firstly done by Taylor and Culick, as mentioned in [5]. The need to gain more insight into propellant flow dynamics led to more research to model and solve such flow. The first research work to reduce a system of equations representing fluid flow inside a chamber to a single ordinary equation using similarity transformation was done by Berman in [6] as stated in works [7,8]. The work done in [9] found that such similarity solutions do not always give acceptable results towards the chamber wall and that instability occurs when no-slip condition is violated.

Similarity transformation was used by [7] to obtain dual solutions of laminar flow inside a non-deformable porous pipe, and that instability of SRM is parameter value-dependent since instability can occur for specific values of parameters affecting the flow. The obtained dual

* Corresponding author.
E-mail addresses: karabomodisep@gmail.com (K. Modise), Gabriel.Magalakwe@nwu.ac.za (G. Magalakwe).

https://doi.org/10.1016/j.tsep.2022.101237
Received 29 July 2021; Received in revised form 12 January 2022; Accepted 10 February 2022
Available online 25 February 2022

Nomenclature

Dimensional Variables

$2a$	Rocket diameter, m
$\dot{a}$	Chamber dilation rate, m/s
$\bar{t}$	Time, s
$\bar{u}$	Velocity along the axial, m/s
$\bar{v}$	Velocity along the radial, m/s
$\bar{z}$	Axial-coordinate, m
$\bar{r}$	Radial-coordinate, m
$\bar{p}$	Flow pressure, Pa
ν	Kinematic viscosity, m^2/s
ρ	Fluid density, kg/m^3
$\bar{\Psi}$	Stream function m^2/s
$\bar{T}$	Fluid temperature, K
$\bar{T}_s$	Temperature at the chamber wall, K
g	Gravitational Acceleration, m/s^2

Non-dimensional Variables

$\bar{t}$	Non-dimensional time
u	Non-dimensional velocity along the axial
v	Non-dimensional velocity along the radial
z	Non-dimensional axial-coordinate
r	Non-dimensional radial-coordinate
A	Wall permeation (injection coefficient)
Ψ	Non-dimensional stream function
α	Non-dimensional chamber wall dilation rate
p	Non-dimensional fluid pressure
Θ	Non-dimensional fluid temperature
Θ_s	Non-dimensional temperature at the chamber wall
R_e	Reynolds number
P_r	Prandtl number
α	Chamber dilation
R	Radiation number
G_r	Grashof number

solutions were found to exist everywhere beside in the domain $2.3 < R_e < 9.1$. In the domain $0 < R_e < 2.3$, the study found that permeation rate $K = 1/R_e$ becomes high such that the system permits at a higher rate, thus resulting reverse flow (instability). On the other hand, when $9.1 < R_e < \infty$ the study found that the system permits at a lower rate, hence leads to well behaved flow. Theoretical and experimental analysis of laminar flow inside a non-deformable porous pipe due to constant injection or suction was done in [10]. In their study, authors found that both analyses gave good results when there is no transverse pressure inside the pipe and the axial pressure increases in the direction of flow for $R_e > 1.25$. The findings in [7,10] revealed that it is not ideal to suck fluid through a non-deformable pipe porous surface at higher rate. These findings in a non-deformable pipe led to an investigation of deformable pipes since deformable pipes have direct application to flow dynamics such as of propellant flow inside the combustion chamber.

The investigation of deformable channels led to the study of important effects such as contraction and expansion. Authors in [11] studied the effects of contraction and expansion on a laminar flow inside a deformable channel and found that the wall shear stress and pressure decrease in the direction of the flow. Saad and Majdalani [12] used perturbation technique to investigate flow inside a deformable channel analytically. The investigation of improved mean-flow inside a deformable pipe to understand rocket motor dynamics was done by [13]. In their study, authors found that the mean flow correlates with the findings in [5] when $R_e = 1000$. The study [14] used Lie symmetry method along with perturbation method to understand how the flow inside a deformable pipe changes with time. The study found that sucking fluid out of the pipe whilst the pipe expands is not desirable since these lead to reverse flow.

The burning of propellant grain to transform the propellant grain to gaseous form introduces heat effects which arise from temperature difference in the system. To understand effects of heat transfer during solid rocket motor operation, a lot of work has been done to gain insight on the influence of parameters that arise from temperature difference such as buoyancy effects, Prandtl number, thermal radiation and convection heat transfer on propellant flow. To know more about the effects of heat transfer during solid rocket motor operation Pearce [15] studied effects of radiation inside rocket combustion chamber. The work in [16] further investigated the effects of radiation on a laminar flow inside a pipe and found that minimal radiation effects weakens fluid convection. Viskanta [17] numerically studied heat convection, fluid heat conduction and radiation effects on a laminar flow.

Furthermore, the effects of interaction between fluid radiation and forced convection on a laminar flow were studied by [18]. The work in [17,18] found that effects of radiation in the axial direction become more when conduction-to-radiation effect is small at the instant temperature is high. Temperature gradient between collection of fluid particles within the fluid bulk leads to variant density, thus introduces a vital parameter of study, namely buoyancy force due to gravity. The propellant burning rate of five percent due to effects of buoyancy force when propellant grain burning surface regression acts against gravity was experimentally obtained by [19]. The influence of buoyancy force and heat on a flow between a pipe which is a rest and circulating pipe was done by [20] numerically.

The SRM propellant sensitivity simulation was conducted on an aluminium particle burn in a gap created between the downward facing combusting and an upward facing inert surface [21]. Authors found that increasing or decreasing the velocity of the propellant surface and propellant surface temperature plume temperature showed greater sensitivity. The study also found that the propellant velocity increases and surface temperature decrease from maximum while the surface gas temperature increases. The authors Griego at el. [21] further studied SRM propellant sensitivity in an upward burning propellant on an aluminium particle combustion simulation using computational fluid dynamics code [22]. The authors found that the propellant velocity increases while surface temperature decreases from maximum while the surface gas temperature increases.

Lie symmetry approach was used by [14] to study the influence of pipe deformation on an unsteady flow inside the pipe without studying thermal parameter effects. In this above mentioned study, solid-propellant rocket stability model and its respective solution account only for velocity (momentum) dynamics, however, this does not represent more realistic Solid Rocket Motor dynamics since the temperature effects play a critical role during rocket operation. Therefore, it is important to have studies that incorporate thermal effects to understand the dynamics of Solid Rocket Motor better. For more realistic rocket dynamics, the current study addresses the impacts of heat distribution during rocket operation to understand the effects of thermal parameters that arise from heat distribution. Incorporating such heat effects has been proposed to address the above shortcoming, thus expand understanding of Solid Rocket Motor operation. The current work aims to deal with the shortcoming in [14], which is to study heat effects since the work in [14] assumed that temperature is constant throughout the chamber during SRM operation. The reason for studying this shortcoming arises from the fact that after SRM ignition, the wall temperature heats propellant inside the SRM chamber, thus diffusion of energy from the wall to the propellant due to temperature difference during operation needs in-depth understanding to understand SRM operation better.

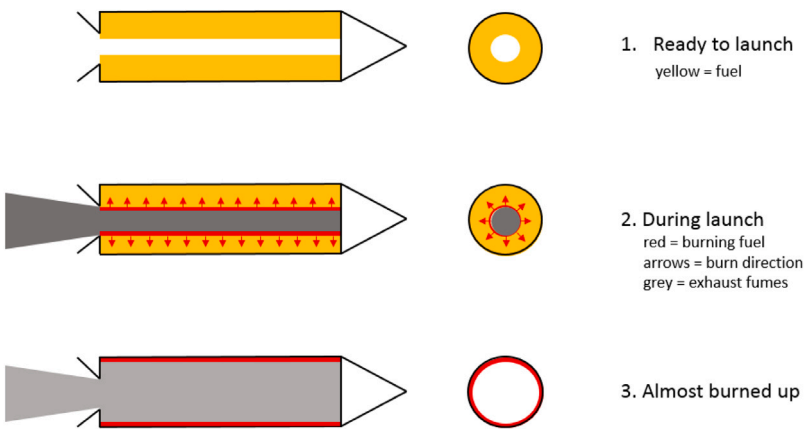

Fig. 1. Flow and heat transfer schematic representation.

Inspired by the work mentioned above, the motivation behind the current study is to improve the work done in [14] by introducing heat, radiation and buoyancy effects on flow the model representing the propellant flow. The current paper aims to find solutions that depend on thermal parameter of the improved flow [14] and heat transfer model representing the propellant flow and heat distribution using Lie symmetry method and perturbation technique. Also, the study seeks to investigate the influence of Reynolds number, chamber expansion, Grashof number, radiation and Prandtl number on a propellant velocity and heat distribution. To obtain optimal steady state operation and a well behaved propellant flow (stable), results are represented graphically, analysed and discussed. The main aim of the study is to highlight thermal parameters values that lead to reverse flow (unstable behaviour) and the ones that lead to stable operation. The study also seeks to give insights of parameters that yields optimal thrust during solid rocket motor operation and well behaved velocity.

2. Mathematical formulation

A two-dimensional unsteady incompressible viscous fluid flow [14] and heat transfer inside a circular semi-infinite pipe is considered. The influence of the heat distribution on the flow studied in [14] is such that thermal effects do not result in any force that leads to momentum change along the transversal direction, hence the current case study is two-dimensional. The pipe wall (chamber wall) is considered porous and its temperature $\bar{T} = \bar{T}_s$ is kept constant. The pipe radius $r = a(t)$ also changes over time, thus the chamber wall expands or contracts equally in the radial direction at a speed of $\dot{a}(t)$. Due to the parabolic behaviour of flow and temperature distribution, the coordinate system is chosen to be symmetric. Fluid is uniformly sucked or injected through the chamber wall, and kinematic viscosity is taken to be constant. In the transverse direction, the internal flow and temperature do not vary, the reader is referred to [1,2] for more information on why it is viable to study two-dimensional flow.

The flow and heat transfer mentioned above is defined by the subsequent cylindrical configuration, as given in Fig. 1

Mathematical representation of the internal flow and heat distribution inside solid rocket motor, is given by

$$\frac{\partial(\bar{r}\bar{u})}{\partial\bar{z}} + \frac{\partial(\bar{r}\bar{v})}{\partial\bar{r}} = 0, \tag{2.1}$$

$$\frac{\partial\bar{u}}{\partial t} + \bar{u}\frac{\partial\bar{u}}{\partial\bar{z}} + \bar{v}\frac{\partial\bar{u}}{\partial\bar{r}} = -\frac{1}{\rho}\frac{\partial\bar{p}}{\partial\bar{z}} + \nu\left[\frac{\partial^2\bar{u}}{\partial\bar{z}^2} + \frac{1}{\bar{r}}\frac{\partial}{\partial\bar{r}}\left(\bar{r}\frac{\partial\bar{u}}{\partial\bar{r}}\right)\right], \tag{2.2}$$

$$\frac{\partial\bar{v}}{\partial t} + \bar{u}\frac{\partial\bar{v}}{\partial\bar{z}} + \bar{v}\frac{\partial\bar{v}}{\partial\bar{r}} = -\frac{1}{\rho}\frac{\partial\bar{p}}{\partial\bar{r}} + \nu\left[\frac{\partial^2\bar{v}}{\partial\bar{z}^2} + \frac{\partial}{\partial\bar{r}}\left(\frac{1}{\bar{r}}\frac{\partial(\bar{r}\bar{v})}{\partial\bar{r}}\right)\right] + g\beta(\bar{T} - \bar{T}_s), \tag{2.3}$$

$$\frac{\partial\bar{T}}{\partial t} + \bar{u}\frac{\partial\bar{T}}{\partial\bar{z}} + \bar{v}\frac{\partial\bar{T}}{\partial\bar{r}} = \lambda\left[\frac{\partial^2\bar{T}}{\partial\bar{z}^2} + \frac{1}{\bar{r}}\frac{\partial}{\partial\bar{r}}\left(\bar{r}\frac{\partial\bar{T}}{\partial\bar{r}}\right)\right] - \frac{1}{\rho c_p}\frac{\partial q_r}{\partial\bar{r}}, \tag{2.4}$$

where $\bar{u}$ and $\bar{v}$ are axial $\bar{z}$ and radial $\bar{r}$ velocity components respectively, $\bar{T}$ is the fluid temperature and $\bar{T}_s$ is wall temperature. Here, ρ is the density, ν is the kinematic viscosity, g is gravitational acceleration, β is thermal expansion coefficient, $\lambda = \frac{k}{\rho c_p}$ is thermal diffusivity, where k is the conductivity of the fluid, c_p is the specific heat, $\bar{p}$ is the fluid pressure, t is time and $q_r = \frac{-4}{3}\frac{\sigma}{k_r}\frac{\partial\bar{T}^4}{\partial\bar{r}}$ is the Roseland approximation, where σ is the Stefan Boltzmann constant and k_r is the Roseland mean absorption coefficient.

According to the design of solid rocket motor, the sufficient boundary conditions are:

$$\begin{aligned}
&\text{(i)}\ \ \bar{u} = 0, \quad \bar{v} = -\bar{v}_s = -V = -\dot{a}A, \quad \bar{T} = \bar{T}_s \quad \text{when } \bar{r} = a(t),\\
&\text{(ii)}\ \ \frac{\partial\bar{u}}{\partial\bar{r}} = 0, \quad \bar{v} = 0, \quad \frac{\partial\bar{T}}{\partial\bar{r}} = 0 \quad \text{when } \bar{r} = 0,\\
&\text{(iii)}\ \ \bar{u} = 0 \quad \text{at } \bar{z} = 0.
\end{aligned} \tag{2.5}$$

In terms of stream function, the components of velocity in the axial and radial directions are

$$\bar{u} = \frac{1}{\bar{r}}\frac{\partial\bar{\Psi}}{\partial\bar{r}} \qquad \text{and} \qquad \bar{v} = -\frac{1}{\bar{r}}\frac{\partial\bar{\Psi}}{\partial\bar{z}}. \tag{2.6}$$

Introducing non-dimensional radial component $r = \bar{r}/a(t)$ into the components (2.6) yields

$$\bar{u} = \frac{1}{a^2 r}\frac{\partial\bar{\Psi}}{\partial r}, \qquad \bar{v} = -\frac{1}{ar}\frac{\partial\bar{\Psi}}{\partial\bar{z}}. \tag{2.7}$$

Substituting (2.7) into Eqs. (2.2), (2.3) and (2.4) along with the following non-dimensional parameters

$$\begin{aligned}
&u = \frac{\bar{u}}{V}, \quad v = \frac{\bar{v}}{V}, \quad z = \frac{\bar{z}}{a(t)}, \ \bar{t} = \frac{tV}{a},\\
&\Psi = \frac{\bar{\Psi}}{a^2 V}, \ p = \frac{\bar{p}}{\rho V^2}, \ \alpha = \frac{a\dot{a}}{\nu}, \ \Theta = \frac{\bar{T} - \bar{T}_s}{T_a - T_s}
\end{aligned} \tag{2.8}$$

yields equations of velocity and equation of energy respectively as

$$r^2\Psi_{r\bar{t}} + r\Psi_r\Psi_{rz} + \Psi_z[\Psi_r - r\Psi_{rr}] + r^3 p_z + \frac{1}{R_e}\Big[(r - \alpha r^3)\Psi_{rr} - r^2\Psi_{rrr} - r^2\Psi_{rzz} - (1 + \alpha r^2)\Psi_r\Big] = 0, \tag{2.9}$$

$$r^2\Psi_{z\bar{t}} + r\Psi_r\Psi_{zz} + \Psi_z[\Psi_z - r\Psi_{rz}] - r^3 p_r + \frac{1}{R_e}\Big[(r - \alpha r^3)\Psi_{rz} - r^2\Psi_{zrr} - r^2\Psi_{zzz}\Big] + r^3 G_r\Theta = 0, \tag{2.10}$$

$$\Theta_{\bar{t}} + \frac{1}{r}\Psi_r\Theta_z - \frac{1}{r}\Psi_z\Theta_r - \frac{1}{P_r R_e}\left[\Theta_{zz} + \frac{\Theta_r}{r} + (1 + 4R)\Theta_{rr}\right] = 0, \tag{2.11}$$

where $\alpha = \frac{a\dot{a}}{\nu}$ is the chamber wall dilation rate, $R_e = \frac{aV_s}{\nu}$ is the Reynolds number, $G_r = \frac{a^3 g\beta(T_a - T_s)}{\nu^2}$ is the Grashof number, $P_r = \frac{\nu\rho c_p}{k}$ is the Prandtl number and $R = \frac{4\sigma T_s^3}{3k_r k}$ is the radiation number.

Similarly, boundary conditions (2.5) become

$$\text{(i) } \Psi_r = 0, \quad \Psi_z = 1, \quad \Theta = 1, \quad \text{when } r = 1,$$
$$\text{(ii) } \left(\frac{\Psi_r}{r}\right)_r = 0, \quad \Psi_z = 0, \quad \Theta_r = 0, \quad \text{when } r = 0,$$
$$\text{(iii) } \Psi_r = 0 \quad \text{at } z = 0. \tag{2.12}$$

The use of (2.8) yields non-dimensional velocity components (2.7) as

$$u = \frac{1}{r}\frac{\partial \Psi}{\partial r} \quad \text{and} \quad v = -\frac{1}{r}\frac{\partial \Psi}{\partial z}. \tag{2.13}$$

3. Solution procedure

This section uses Lie symmetry analysis [23–27] to find similarity transformation and use them to transform Eqs. (2.9)–(2.12) to ordinary differential equations. Perturbation method is further used to obtain semi-analytical solutions representing the internal velocity and temperature distribution during steady operation.

3.1. Lie symmetry analysis

The dimensionless system (2.9)–(2.11) representing solid rocket motor operation admits the following five symmetries:

$$X_1 = z\left(2K\alpha e_5'(\bar{t}) - e_5''(\bar{t})\right)\frac{\partial}{\partial p} + \frac{r^2}{2}e_5'(\bar{t})\frac{\partial}{\partial \Psi} - z\frac{\partial}{\partial z}, \quad X_2 = \frac{\partial}{\partial \bar{t}},$$
$$X_3 = a_7(\bar{t})\frac{\partial}{\partial \Psi}, \quad X_4 = b_4(\bar{t})\frac{\partial}{\partial p}, \quad X_5 = rG_r\frac{\partial}{\partial p} + \frac{\partial}{\partial \Theta}.$$

The operator X_2 is the only Lie symmetry that maintains the steady state dynamics of the system if

$$\Phi_\Psi = X(\Psi) = 0, \quad \text{where} \quad \Psi = \Psi(z, r, \bar{t}), \tag{3.14}$$

$$\Phi_P = X(p) = 0, \quad \text{where} \quad p = p(z, r, \bar{t}) \tag{3.15}$$

and

$$\Phi_\Theta = X(\Theta) = 0, \quad \text{where} \quad \Theta = \Theta(z, r, \bar{t}), \tag{3.16}$$

where X is Lie symmetry operator. It follows from this symmetry that

$$\Phi_\Psi = -\Psi_{\bar{t}}, \quad \Phi_p = -p_{\bar{t}}, \quad \Phi_\Theta = -\Theta_{\bar{t}} \tag{3.17}$$

are invariant under X_2.

Thus, according to (3.17), the steady state solutions for velocity, pressure and temperature are respectively

$$\Psi = h(r)N(z, r), \quad p = \Gamma(z, r) \quad \text{and} \quad \Theta = \omega(z, r). \tag{3.18}$$

Using steady state solutions (3.18) into (2.9) and taking

$$K_1 = N_z, \quad K_2 = \frac{N_r}{N}, \quad K_3 = \frac{N_z N_r}{N}, \quad K_4 = \frac{N_{zz}}{N},$$
$$K_5 = \frac{N_{rr}}{N}, \quad K_6 = \frac{N_{rzz}}{N},$$
$$K_7 = \frac{N_{rrr}}{N}, \quad K_8 = N_{rz}, \quad K_9 = \frac{N_r N_{rz}}{N},$$
$$K_{10} = \frac{N_z N_{rr}}{N}, \quad K = \frac{1}{R_e}, \tag{3.19}$$

yields

$$-r^2K\frac{d^3h}{dr^3} + \left[-rhK_1 + Kr - \alpha Kr^3 - 3Kr^2K_2\right]\frac{d^2h}{dr^2}$$
$$+ \left[hK_1 - rhK_3 + 2K(r - \alpha r^3)K_2 - 3Kr^2K_5 - Kr^2K_4\right.$$
$$\left. - K - \alpha Kr^2 + rhK_8\right]\frac{dh}{dr}$$
$$+ rK_1\left(\frac{dh}{dr}\right)^2 + \left[K(r - \alpha r^3)K_5 - Kr^2K_7 - Kr^2K_6 - K(1 + \alpha r^2)K_2\right]h$$
$$+ \left[rK_9 + K_3 + rK_{10}\right]h^2 + \frac{r^3}{N}\frac{\partial \Gamma}{\partial z} = 0. \tag{3.20}$$

Integrating the first equation of system (3.19) with respect to z, yields

$$N(z, r) = zK_1(r) + K_{11}(r). \tag{3.21}$$

The stream function (3.18) in terms of the above value of $N(z, r)$ becomes

$$\Psi = \left[zK_1(r) + K_{11}(r)\right]h(r). \tag{3.22}$$

Differentiating the above Eq. (3.22) with respect to r and thereafter using the stream function condition from (2.12) (iii), gives

$$K_{11}(r)h(r) = K_{12}, \tag{3.23}$$

where K_{12} is a constant of integration.

Invoking K_{12} given by (3.23) into stream function (3.22) gives

$$\Psi = zG(r) + K_{12}, \tag{3.24}$$

here $G(r) = K_1(r)h(r)$.

Using pressure $p = \Gamma(r, z)$ from (3.18) for state operation and non-dimensional stream function (3.24) into (2.9), yields

$$r^3\frac{\partial \Gamma}{\partial z} = z\left[\left\{(1 + \alpha r^2)K - G\right\}\frac{dG}{dr} + \left\{rG - (r - \alpha r^3)K\right\}\frac{d^2G}{dr^2}\right.$$
$$\left. - r\left(\frac{dG}{dr}\right)^2 + r^2K\frac{d^3G}{dr^3}\right]. \tag{3.25}$$

The use of (3.21) and (3.25) into (3.20) yields

$$K_{11} = 0, \tag{3.26}$$

thus, the velocity (3.21) becomes

$$\Psi(z, r) = zK_1(r). \tag{3.27}$$

Since K_{11} is zero, K_{12} is also zero from (3.23), thus Eq. (3.24) becomes

$$\Psi = zG(r). \tag{3.28}$$

Substituting (3.28) into (2.13) gives the following propellant velocity components

$$\frac{u}{z} = \frac{1}{r}\frac{dG}{dr} \quad \text{and} \quad v = -\frac{G}{r}. \tag{3.29}$$

The results above indicate that the flow is laminar since both the radial velocity and the axial velocity per length z depend on r only.

Using the steady state temperature (3.18) and stream function (3.28) into (2.10) and differentiating the resulting equation with respect to z, yields pressure variation as

$$p_{rz} = G_r\omega_z. \tag{3.30}$$

Differentiating the axial momentum equation obtained from using (3.28) with respect to r and thereafter substituting pressure from (3.30) yields

$$K\left[r^2\frac{d^4G}{dr^4} + (\alpha r^3 - 2r)\frac{d^3G}{dr^3} + (\alpha r^2 + 3)\frac{d^2G}{dr^2} - \left(\alpha r + \frac{3}{r}\right)\frac{dG}{dr}\right] - r\frac{dG}{dr}\frac{d^2G}{dr^2}$$
$$+ \left(\frac{dG}{dr}\right)^2 - 3G\frac{d^2G}{dr^2} + \frac{3}{r}G\frac{dG}{dr} + rG\frac{d^3G}{dr^3} - \frac{r^3G_r\omega_z}{z} = 0. \tag{3.31}$$

The above Eq. (3.31) gives third derivative of temperature as

$$r^3G_r\omega_{zzz} = 0. \tag{3.32}$$

There are effects of buoyancy force, thus based on the dynamics of the propellant, G_r is a non-zero parameter and radius is also not zero, consequently, $\omega_{zzz} = 0$, which yields

$$\omega_{zz} = F_1(r), \tag{3.33}$$

where the function $F_1(r)$ depends on r. Integrating (3.33) with respect to z gives

$$\omega_z = zF_1(r) + F_2(r), \tag{3.34}$$

where the function $F_2(r)$ depends on r. The headwall is insulated according to the design, thus at the headwall, there is no transfer of heat, hence $\omega_z = 0$ at $z = 0$, so (3.34) yields $F_2(r) = 0$. It follows that temperature variation per length is such that

$$\frac{\omega_z}{z} = F_1(r), \tag{3.35}$$

which is evident that the temperature from the rocket chamber wall only influences the propellant along the radial direction, so there is no heat diffusion along the axial direction. Thus Eq. (3.35), yields $\frac{\omega_{zz}}{z} = 0$.

Since there is no axial heat diffusion according to the design, by using components (3.29) and temperature (3.35) into (3.31) and (2.11) respectively while letting temperature variation $F_1(r) = H(r)$ from (3.35), yields velocity and energy equations as

$$K\left[2\beta\frac{d^4G}{d\beta^4} + (2\alpha\beta + 4)\frac{d^3G}{d\beta^3} + 4\alpha\frac{d^2G}{d\beta^2}\right] + G\frac{d^3G}{d\beta^3} - \frac{dG}{d\beta}\frac{d^2G}{d\beta^2} - \frac{HG_r}{\sqrt{2\beta}} = 0, \tag{3.36}$$

$$\frac{dG}{d\beta}H - \frac{G}{2}\frac{dH}{d\beta} - \frac{K}{P_r}\left[\frac{dH}{d\beta} + \beta\frac{dH^2}{d\beta^2}\right] - \frac{2RK}{P_r}\left[\frac{dH}{d\beta} + 2\beta\frac{dH^2}{d\beta^2}\right] = 0, \tag{3.37}$$

where $\frac{r^2}{2} = \beta$. Similarly, the conditions at the boundary yields

$$\text{(i) } \frac{dG(1/2)}{d\beta} = 0,\ \text{(ii) } G(1/2) = 1,\ \text{(iii) } G(0) = 0,$$
$$\text{(iv) } \lim_{\beta\to 0}\sqrt{2\beta}\,\frac{d^2G}{d\beta^2} = 0,\ \text{(v) } H(1/2) = 1,\ \text{(vi) } \frac{dH(0)}{d\beta} = 0. \tag{3.38}$$

3.2. Analytical solutions

This section uses perturbation method [14], to solve the fourth-order differential Eq. (3.36) representing the flow and the second-order differential Eq. (3.37) representing heat distribution inside a rocket chamber. Since the current study investigates the effects of thermal parameters on the propellant flow velocity, the perturbation method allows one to choose thermal parameters as perturbation quantities that yield solutions that depend on those thermal parameters. Also, this method linearise coupled system of equations representing the case study.

The rocket is designed in such a way that it allows weak propellant injection through the surface wall, thus that $K = \frac{1}{R_e}$ is minimal and the fluid density variation is such that the Gr effects are minimal. Thus, the flow velocity G and internal temperature H can be expressed in a series form in terms of those small parameters as

$$G = G_1 + KG_2 + O(K^2), \qquad H = H_1 + KH_2 + O(K^2), \tag{3.39}$$

where the zero-th order terms G_1, H_1 and first order terms G_2, H_2 of K are given by equations

$$G_1 = G_{10} + G_rG_{11} + O(G_r^2), \qquad H_1 = H_{10} + G_rH_{11} + O(G_r^2),$$
$$G_2 = G_{20} + G_rG_{21} + O(G_r^2), \qquad H_2 = H_{20} + G_rH_{21} + O(G_r^2) \tag{3.40}$$

respectively.

Substituting the velocity G, temperature H from (3.39), zero-th order and first order terms (3.40) into Eqs. (3.36) and (3.37) yield a system of eight equations and appropriate boundary conditions by equating powers of the perturbation quantities K and G_r. The solutions of the resulting system of equations yield two solutions representing momentum variation and temperature distribution inside the combustion chamber as follows:

$$\begin{aligned}
G =\ & \sin\theta + G_r\Big[0.02\sqrt{\theta}\big[\sin\theta - \theta\cos\theta\big] + I_1\sin\theta \\
& + \cos\theta\big[\theta I_2 + I_3 + I_4 + I_5\big] + a_1\sin\theta + a_2\theta\cos\theta + a_3\cos\theta\Big] \\
& + K\left[\frac{\alpha}{\pi}\big[3\ln\tan(\theta/2)(\sin\theta - \theta\cos\theta) - 2\theta\big] - 3 + (\theta\cos\theta - \sin\theta)I_6\right. \\
& + \Big(\frac{3\alpha}{\pi}I_6 - I_7\Big)\cos\theta + b_1\sin\theta + b_2\theta\cos\theta + b_3\cos\theta \\
& + G_r\Big\{\sin\theta\Big[-1.7348\times10^{-18}\alpha\big(\cos\theta - \ln[\cos(\theta/2)] \\
& + \ln[\sin(\theta 2)]\big) + A_1 \\
& + 4.3368\times10^{-18}\big(\cos\theta - \ln[\cos(\theta/2)] + \ln[\sin(\theta/2)]\big) + j_1\Big] \\
& + \theta\cos\theta\Big[-1.7348\times10^{-18}\alpha\big(\cos\theta - \ln[\cos(\theta/2)] + \ln[\sin(\theta/2)]\big) \\
& + A_2 - 4.3368\times10^{-18}\alpha\big(\cos\theta - \ln[\cos(\theta/2)] + \ln[\sin(\theta/2)]\big) + j_2\Big] \\
& \left. + \cos\theta(A_3 + j_3)\Big\}\right]
\end{aligned} \tag{3.41}$$

and

$$\begin{aligned}
H =\ & -\frac{\cos 2\theta}{2} + \frac{1}{2} + G_r\big[3.49232\times10^{17}\big(\theta^2 - 0.059607\theta^{\frac{5}{2}} - 0.128479\theta^{\frac{7}{2}}\big)\big] \\
& + K\left\{\frac{2}{\pi P_r}\Big(4\pi\theta + 12\pi R\theta - 8\theta^2 - 24R\theta^2 + \pi^2\theta^2P_r - 2\pi\theta^3P_r\Big)\right. \\
& + G_r\Big[\frac{2.77556\times10^{-16}}{P_r\theta^3}\Big(3.96584\times10^{14}\theta^4 + 1.18975\times10^{15}R\theta^4 \\
& + 0.725\theta^{4.5} + 4.8R\theta^{4.5} \\
& - 2.52473\times10^{14}\theta^5 - 7.57419\times10^{14}R\theta^5 + 16.6568\theta^{5.5} \\
& + 7.10985R\times10^{5.5} + 2\theta^6 - 0.4R\theta^6 \\
& + 0.0823318\theta^{6.5} + 0.4\theta^5\ln\theta + 7.80626\times10^{-19}\theta^{3.5}P_r \\
& + 0.125\theta^4P_r + 0.246995R\theta^{6.5} \\
& + 3.11476\times10^5P_r - 2.38917\theta^{5.5}P_r - 1.98292\times10^{14}\theta^6P_r \\
& + 0.0661165\theta^{6.5}P_r \\
& + 0.0323316\theta^{7.5}P_r - 1.249\times10^{-17}\times\theta^{3.5}\alpha P_r - 1.96906\theta^{5.5}\alpha P_r \\
& - 0.5\theta^6\alpha P_r + 0.00666862\theta^{6.5}\alpha P_r \\
& + 1.50303\times10^{-16}\theta^5\ln\theta P_r + 2.22045\times10^{-17}\theta^{5.5}\ln\theta P_r \\
& \left.\left. - 3.75759\times10^{-17}\theta^5\alpha\ln\theta P_r\Big)\Big]\right\}.
\end{aligned} \tag{3.42}$$

When Grashof number becomes minimal the velocity solution (3.41) turn to the one obtained in [14], which should be the case since the current study is an extension of [14].

See the appendix for values $I_1, \ldots, I_{41}$, which arise when solving velocity (3.41). The series forms of non-integrable functions $I_1, \ldots, I_{41}$ are given in Appendix A, and integration constants $a_1, a_2, a_3, b_1, b_2, b_3, j_1, j_2$ and j_3 are given in Appendices B and C respectively.

The velocity components (3.29) can be rewritten as β

$$u/z = G_\beta \qquad \text{and} \qquad v = -G/\sqrt{2\beta}. \tag{3.43}$$

Substituting (3.28) into (2.10) yields pressure drop in the radial direction as

$$p_\beta = \left[-\frac{G^2}{(2\beta)^2} - \frac{GG_\beta}{2\beta} - \alpha KG_\beta - KG_{\beta\beta}\right] + \frac{G_rH}{\sqrt{2\beta}}. \tag{3.44}$$

The distribution of pressure in the radial direction is obtained by integrating (3.44) together with (3.38) and while taking p_c to be the centreline and p_β surface pressure respectively, thus

$$\int_{p_c}^{p_\beta} dp = -\int_0^\beta\left[-\frac{G^2}{(2\beta)^2} - \frac{GG_\beta}{2\beta} - \alpha KG_\beta - KG_{\beta\beta}\right]d\beta + \int_0^\beta\frac{G_rH}{\sqrt{2\beta}}d\beta. \tag{3.45}$$

Thus, the axial pressure drop is

$$\begin{aligned}
\Delta p_r &= p_\beta - p_c, \\
&= KG_\beta(0) - \left[\frac{1}{\beta}\left(\frac{G}{2}\right)^2 + \alpha KG + KG_\beta\right] + \chi,
\end{aligned} \tag{3.46}$$

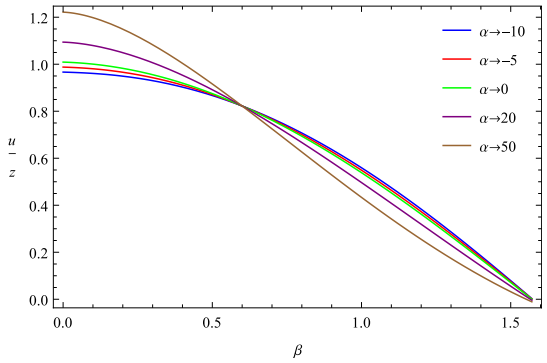

Fig. 2. Influence of α on velocity when $K = 0.01$, $P_r = 6$, $R = 10$ and $G_r = 0.02$.

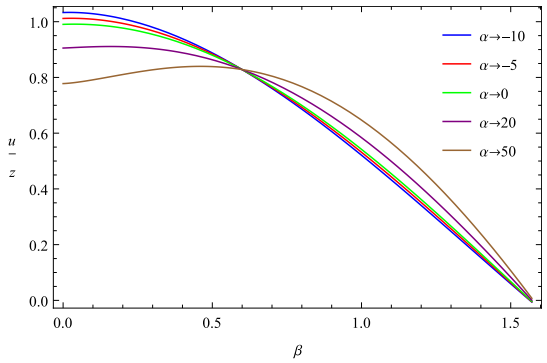

Fig. 3. Influence of α on velocity when $K = -0.01$, $P_r = 6$, $R = 10$ and $G_r = 0.02$.

where $\chi = \int_0^{\beta} \frac{G_r H}{\sqrt{2\beta}} d\beta$. This component indicates the buoyancy force contribution to the system radial pressure inside the combustion chamber.

4. Results and discussion

Graphical representations of flow velocity per length u/z and internal temperature H are given in this section. Analysis of various parameters which influence flow velocity and internal temperature respectively is carried out to better understand the steady state operation of solid rocket motor.

4.1. Velocity profiles under the influence of dimensionless parameters that affect velocity and heat distribution

In this subsection, the impact of different parameters on propellant flow velocity are analysed.

4.1.1. Influence of chamber dilation α on the velocity

Fig. 2 shows the influence of chamber dilation on velocity for injection $K = 0.01$. When combustion chamber volume increases ($\alpha > 0$), propellant (fluid) velocity increases close to the middle of the chamber (centre) while it decreases close to the chamber wall. This finding is attributed to the additional volume created by expansion while fluid injected through the chamber wall fill up the additional chamber space, thus net work done leads to positive work within the chamber. The decrease in chamber volume ($\alpha < 0$), results in positive work performed by chamber wall and fluid injection, such that the internal net work done is more towards the chamber wall and low towards the centre. Thus, the internal flow velocity increases towards the chamber wall and decreases towards the middle of the chamber due to this net work done.

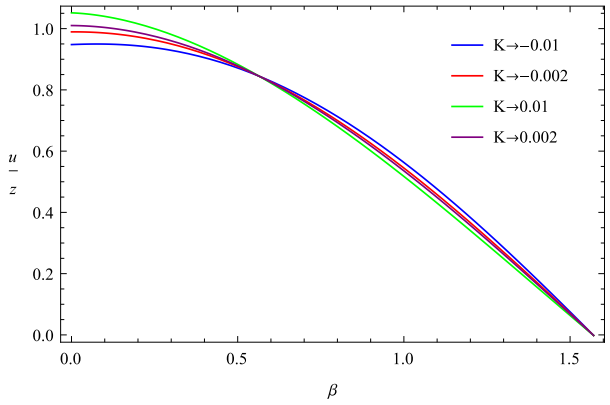

Fig. 4. Influence of K on velocity when $\alpha = 10$, $P_r = 6$, $R = 10$ and $G_r = 0.02$.

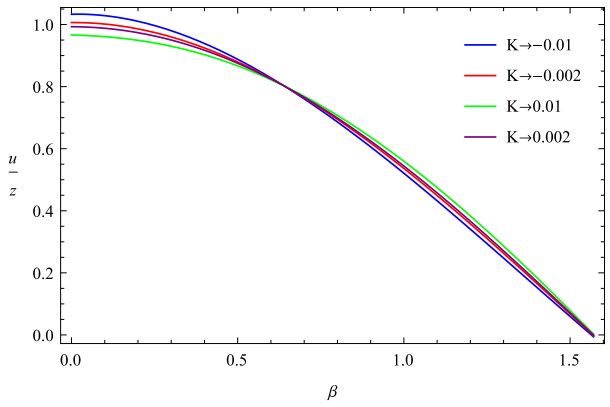

Fig. 5. Influence of K on velocity when $\alpha = -10$, $P_r = 6$, $R = 10$ and $G_r = 0.02$.

In the case of wall contraction and fluid suction, it is found that the decrease in chamber space contributes to a higher fluid velocity at the centre and lower towards the chamber wall. The high fluid velocity is due to the reduction in volume, which increases pressure in the outflow direction, as shown in Fig. 3. According to Fig. 2 and the velocity is more for flow injection than for flow suction.

4.1.2. Influence of Reynolds number K on the velocity

For fluid injection ($K > 0$), Fig. 4 shows that the velocity inside the combustion chamber becomes high at the centre and low toward the chamber wall while the chamber volume increases. Also, Fig. 4 shows that sucking fluid through the surface ($K < 0$), while chamber volume increase leads to negative work done, thus flow velocity decrease towards the centre and increase towards the chamber wall. This observation is caused by the additional space that increases flow towards the wall, thus decrease the flow towards the rockets nozzle, leading to the decrease in thrust.

In the case of fluid injection, when ($K > 0$) while the chamber internal space decreases ($\alpha < 0$), Fig. 5 shows that the flow velocity decreases towards the centre and increases towards the chamber wall. This behaviour is caused by the decrease in volume, which increases internal friction such that particles free movement decreases inside the chamber, thus reducing thrust during solid rocket motor operation. Fig. 5 indicates that sucking fluid out of the combustion chamber while the chamber volume decreases lead to an increase in velocity towards the centre and velocity decrease towards the chamber wall. This behaviour is caused by a decrease in particles closed to the chamber wall due to sucking.

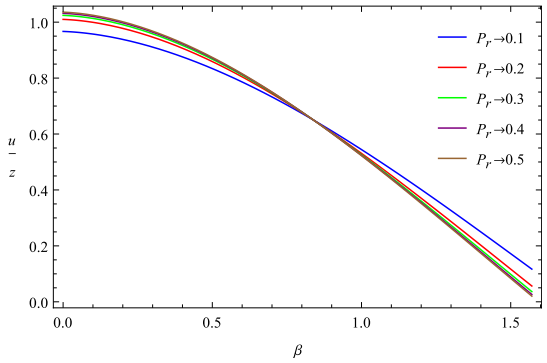

Fig. 6. Influence of P_r on velocity when $\alpha = 10$, $G_r = 0.02$, $R = 10$ and $K = 0.01$.

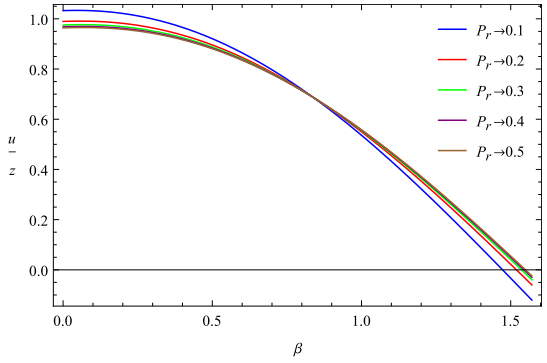

Fig. 7. Influence of P_r on velocity when $\alpha = 10$, $G_r = 0.02$, $R = 10$ and $K = -0.01$.

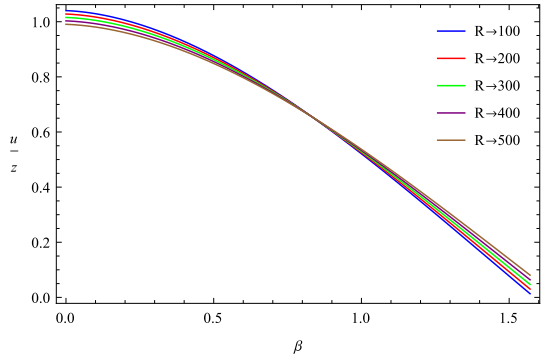

Fig. 8. Influence of R on velocity when $\alpha = 10$, $G_r = 0.02$, $K = 0.01$ and $P_r = 6$.

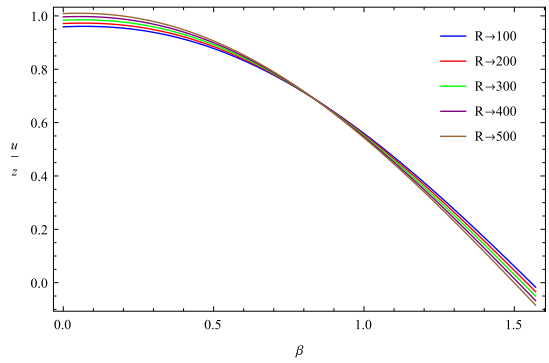

Fig. 9. Influence of R on when $\alpha = 10$, $G_r = 0.02$, $K = -0.01$ and $P_r = 6$.

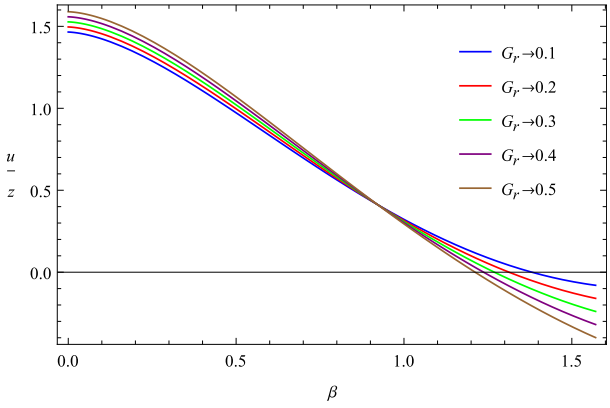

Fig. 10. Influence of G_r on velocity when $K = 0.01$, $P_r = 2$, $R = 10$ and $\alpha = 50$.

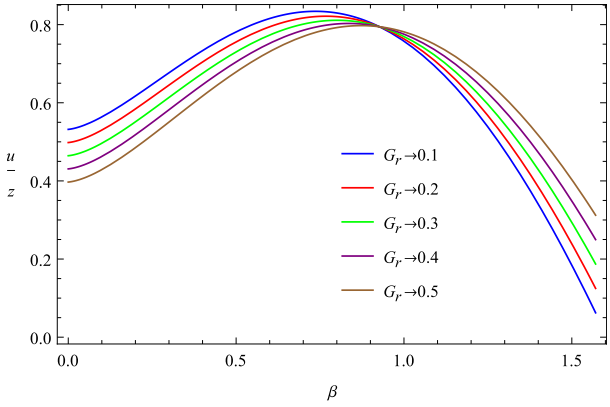

Fig. 11. Influence of G_r on velocity when $K = -0.01$, $P_r = 2$, $R = 10$ and $\alpha = 50$.

4.1.3. Influence of Prandtl number on the velocity

Fig. 6 shows that the increase in Prandtl number P_r when fluid is injected inside the chamber leads to an increase in velocity towards the centre and a decrease in velocity towards the chamber wall. However, Fig. 7 illustrates that the increase in Prandtl number decreases flow velocity towards the chamber centre and increase flow velocity toward the chamber wall. These behaviours are caused by a decrease in fluid density due to heat diffusion, allowing fluid to flow easily. Hence, fluid injection or fluid suction (in or out of the chamber) happens quicker when fluid is less dense.

4.1.4. Influence of radiation on velocity

Fig. 8 shows that increasing radiation R when fluid is injected inside the chamber, leads to a decrease in velocity towards the centre and an increase in velocity towards the wall. This phenomenon arises from the dominance of momentum diffusivity $P_r = 6$ over thermal diffusivity, thus the fluid injected inside the chamber creates internal friction which results in more fluid particles absorbing radiation. However, Fig. 9 illustrates that radiation increases flow velocity towards the chamber centre and decreases flow velocity toward the chamber wall. This behaviour is caused by the fact that more radiative particles will be sucked and decrease the number of particles inside the chamber, thus decreasing friction.

4.1.5. Influence of Grashof number on the velocity

Fig. 10 shows that the increase in Grashof number when fluid is injected inside the chamber increases the flow velocity towards the centre and decrease the flow velocity towards the wall. This phenomenon is caused by gravity, which causes more dense fluid particles to move to the bottom and the less dense fluid particles sideways in the axial direction. Thus this movement of particles towards the bottom causes

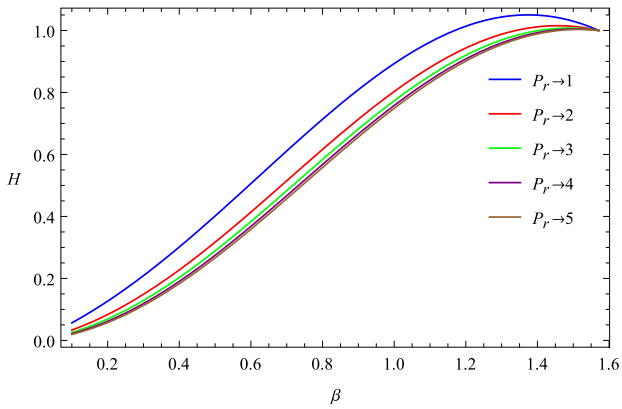

Fig. 12. Influence of P_r on temperature when $K = 0.002$, $R = 10$, $\alpha = 5$ and $G_r = 0.02$.

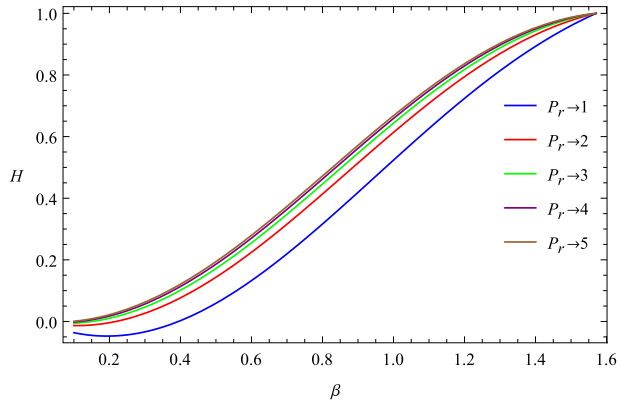

Fig. 13. Influence of P_r on temperature when $K = -0.002$, $R = 10$, $\alpha = 5$ and $G_r = 0.02$.

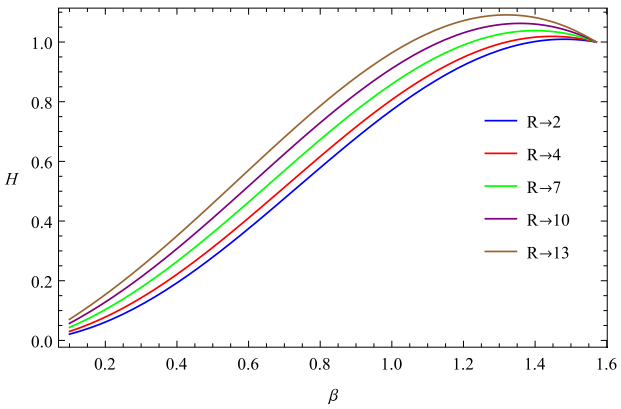

Fig. 14. Influence of R on temperature when $K = 0.002$, $\alpha = 5$, $P_r = 6$ and $G_r = 0.02$.

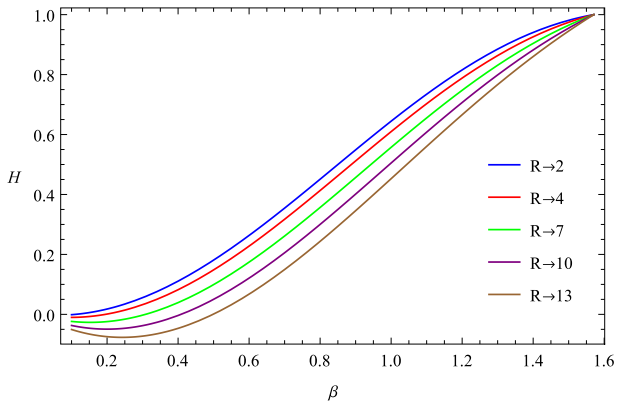

Fig. 15. Influence of R on temperature when $K = -0.002$, $\alpha = 5$, $P_r = 6$ and $G_r = 0.02$.

reverse flow at the wall which lead to instability. However, Fig. 11 illustrates that the increase in Grashof number when fluid is sucked decreases flow velocity towards the chamber centre and increase flow velocity towards the chamber wall. The velocity decrease is due to gravitational force, which causes dense fluid particles to move towards centre and less dense particles to move towards the chamber wall.

4.2. Effects of dimensionless parameters on temperature distribution

In this subsection, the impact of various parameters on propellant temperature distribution are analysed during solid rocket motor operation.

4.2.1. Influence of Prandtl number on temperature

Fig. 12 shows that the decrease in Prandtl number P_r increases temperature when fluid is injected inside the chamber. The rise in temperature during injection is because when the Prandtl number decreases, momentum diffusivity (velocity) decreases while thermal diffusivity increases (heat conduction), thus heat conduction and temperature inside the chamber increase. The slight energy increment close to the chamber wall gives the propellant energy to move towards the centre. Fig. 13, on the other hand, shows that the increase in Prandtl leads to a temperature rise when fluid is sucked out of the chamber. Sucking fluid out of the chamber increasing thermal diffusivity, thus increasing heat conduction. This indicates that internal temperature increases more for high Prandtl number when fluid is sucked.

4.2.2. Influence of radiation on temperature

Fig. 14 shows that the internal temperature increases with radiation when fluid is injected inside the chamber. This observation is caused by additional temperature in the form of radiation which increases internal temperature. Also, the internal temperature decreases towards the centre, since the rocket loses energy in the form of thrust at the centre during operation. Fig. 15 indicates that the temperature decreases with an increase in radiation, since the particles sucked through the surface out of the chamber leads to a decrease in internal temperature when energy is sucked out in the form of radiation.

4.2.3. Influence of Reynolds number on temperature

Figs. 16 and 17 show that temperature increases with fluid injection for both contracting and expanding chambers. The increase in temperature is caused by increased in momentum when more particles are injected inside the chamber. Also, during suction, momentum decreases with the decrease in fluid particles, thus decreasing the temperature inside the chamber.

4.2.4. Influence of Grashof number on temperature

Fig. 18 shows that the internal temperature increases with the increase in Grashof number when fluid is injected inside the chambers. This increase in temperature is due to the high Grashof number, which results from high heat diffusion, thus increasing heat transfer and internal temperature. Fig. 19 indicates that when fluid is sucked through the surface out of the chamber, temperature decreases with the increase in Grashof number. The decrease in temperature during suction arises because the fluid particles sucked through the surface

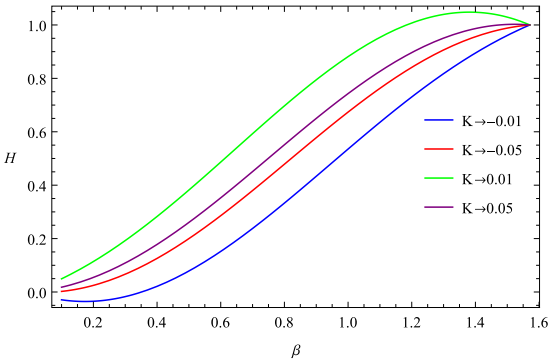

Fig. 16. Influence of K on temperature when $R = 10$, $\alpha = 5$, $P_r = 6$ and $G_r = 0.02$.

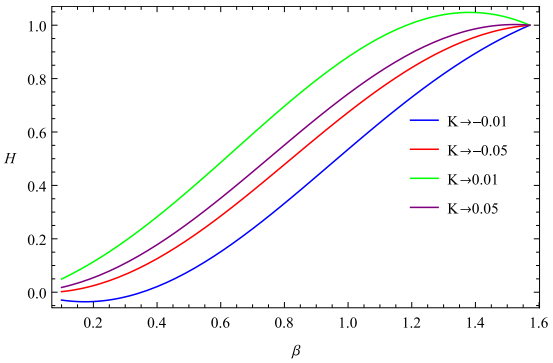

Fig. 17. Influence of K on temperature when $R = 10$, $\alpha = -5$, $P_r = 6$ and $G_r = 0.02$.

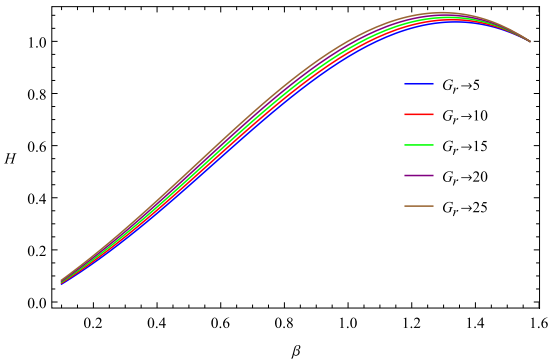

Fig. 18. Influence of G_r on temperature when $K = 0.002$, $R = 10$, $\alpha = 5$, $P_r = 6$.

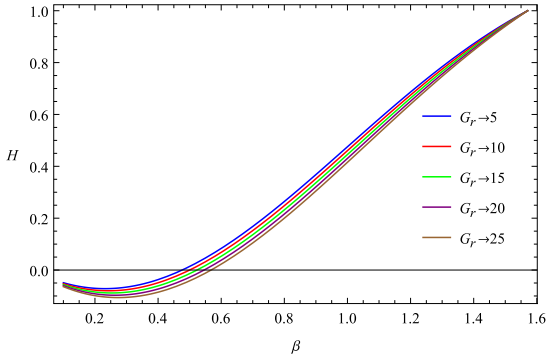

Fig. 19. Influence of G_r when $K = -0.002$, $R = 10$, $\alpha = 5$, $P_r = 6$.

possess high temperatures for high Grashof, thus removing heat from the chamber.

5. Conclusion and remarks

To better explain the dynamics of SRM stability, this paper further advance the subject of viscous incompressible fluid flow in a cylindrical deformable porous pipe by further studying the work in [14]. Lie symmetry analysis was used in combination with the double perturbation expansion approach to obtain semi-analytical solutions to the problem at hand. The study mainly shows that internal temperature and thermal parameters arising from the system affects the momentum, thus influence thrust during operation. The study indicates that for Prandtl number values $Pr > 0.1$, sucking propellant out of the combustion chamber leads to propellant velocity flow field instabilities, but leads to stable operation during injection. The study also shows Grashof number values $G_r > 0.1$ while injecting propellant into the combustion leads to unstable propellant velocity field but stable flow velocity during suction. Also, injecting fluid inside the chamber increases internal energy, thus increasing work done. The flow velocity solution [14] was also retrieved by letting the Grashof number to be zero in the solution obtained for momentum, which should be the case since the current study is an extension of [14]. The obtained flow velocity and internal temperature profiles are similar to those in the literature. The obtained parabolic velocity profiles which can be attributed to no-slip conditions are similar to the ones obtained in [28,29]. The marginally S formed internal temperature profile attributed to intense convective motion similar to the results in [30–32], which brings hot combustion products in a circular pipe closer to the pipe centre, were obtained. The current work offers further insight into the dynamics that contributes to stable operation of SRM studied in [14] by illustrating that temperature must be configured in such a way that the effects of buoyancy must be minimal since high temperature contributes to greater buoyancy force effect, which is not desirable for SRM as it results in reverse flow, thus decrease propulsion. For a system to obtain the steady state regime operation, the following results are critical:

- **Wall Dilation**: The volume chamber needs to decrease during operation to crate effective pressure while the system injects fluid to obtain optimal solid rocket motor thrust.
- **Reynolds number**: Fluid injection is ideal, while suction is not ideal, so propellant injection inside the rocket chamber is required to optimise thrust during operation.
- **Prandtl number**: The internal temperature rise resulting from the increase in the Prandtl number is ideal during operation as the temperature increase leads to an increase in the system's internal energy and the work done to propel, thus maximise the thrust.
- **Radiation Number:** Increasing radiation in the system increases in internal energy, thus increase the work done to propel and this increase in radiation is needed to improve thrust during operation.
- **Grashof number:** The work performed by the buoyancy effect needs to raise the system's internal energy such that the work done internally leads to an increase thrust.

To understand the dynamics of solid rocket motor operation better, in future one can study the transition from steady-state regime to unsteady state regime and study the dynamics of Solid Rocket Motor in three-dimension by including the analysis of momentum variation in the transverse direction. Also, the vorticity effects on the flow and heat distribution can be investigated.

Declaration of competing interest

The authors declare that they have no known competing financial interests or personal relationships that could have appeared to influence the work reported in this paper.

Acknowledgements

For financial assistance, the authors would like to thank CSIR, Republic of South Africa and the North-West University South Africa.

Appendix A. Non-integrable functions

$$I_1 = \int_0^{\theta} \frac{-0.01\cos^2\theta\cos 2\theta}{\sqrt{\theta}}d\theta$$

$$I_2 = \int_0^{\theta} \frac{0.01\cos 2\theta}{\sqrt{\theta}}d\theta, \quad I_3 = \int_0^{\theta} -0.01\sqrt{\theta}\cos 2\theta d\theta$$

$$I_4 = \int_0^{\theta} \frac{0.01\sin\theta\cos 2\theta\cos\theta}{\sqrt{\theta}}d\theta$$

$$I_5 = \int_0^{\theta} \frac{-0.01\sin\theta\cos\theta}{\sqrt{\theta}}d\theta$$

$$I_6 = \int_0^{\theta} \theta\mathrm{cosec}\theta\, d\theta, \quad I_7 = \int_0^{\theta} \theta^2\mathrm{cosec}\theta\, d\theta$$

$$I_8 = \int_0^{\theta} \frac{-\cos^2\theta}{2\sin\theta}\frac{0.9709R}{P_r\sqrt{\theta}}d\theta$$

$$I_9 = \int_0^{\theta} \frac{1.1654\times10^{-17}\cos^2\theta}{2\sin\theta\sqrt{\theta}}d\theta$$

$$I_{10} = \int_0^{\theta} \frac{-\cos^2\theta}{2\sin\theta}\frac{0.32337}{P_r\sqrt{\theta}}d\theta,\ I_{11} = \int_0^{\theta} \frac{-0.7875\cos^2\theta}{2\sin\theta\sqrt{\theta}}d\theta$$

$$I_{12} = \int_0^{\theta} \frac{3.0791\times10^{-18}\alpha\cos^2}{2\sin\theta\theta^{\frac{3}{2}}}d\theta$$

$$I_{13} = \int_0^{\theta} \frac{-2.8112\times10^{-19}\cos^2}{2\sin\theta\theta^{\frac{3}{2}}}d\theta$$

$$I_{14} = \int_0^{\theta} \frac{-2.2446\times10^{-34}\alpha\theta\cos^2\theta}{2\sin\theta}d\theta$$

$$I_{15} = \int_0^{\theta} \frac{-0.2556\alpha\sqrt{\theta}\cos^2\theta}{2\sin\theta}d\theta$$

$$I_{16} = \int_0^{\theta} \frac{0.6176R\sqrt{\theta}\cos^2\theta}{2\sin\theta P_r}d\theta$$

$$I_{17} = \int_0^{\theta} \frac{-1.8498\times10^{-17}\sqrt{\theta}\ln\theta}{2\sin\theta}d\theta$$

$$I_{18} = \int_0^{\theta} \frac{2.0586\sqrt{\theta}\cos^2\theta}{2\sin\theta P_r}d\theta$$

$$I_{19} = \int_0^{\theta} \frac{-0.3114\sqrt{\theta}\cos^2\theta}{2\sin\theta}d\theta$$

$$I_{20} = \int_0^{\theta} \frac{0.97091R}{2P_r\sin\theta\sqrt{\theta}}d\theta$$

$$I_{21} = \int_0^{\theta} \frac{-1.1654\times10^{-17}}{2\sin\theta\sqrt{\theta}}d\theta$$

$$I_{22} = \int_0^{\theta} \frac{0.32337}{2P_r\sin\theta\sqrt{\theta}}d\theta$$

$$I_{23} = \int_0^{\theta} \frac{0.7875}{2\sin\theta\sqrt{\theta}}d\theta$$

$$I_{24} = \int_0^{\theta} \frac{-3.079\times10^{-18}\alpha}{2\sin\theta\theta^{\frac{3}{2}}}d\theta$$

$$I_{25} = \int_0^{\theta} \frac{2.8112\times10^{-19}}{2\sin\theta\theta^{\frac{3}{2}}}d\theta$$

$$I_{26} = \int_0^{\theta} \frac{2.2446\times10^{-34}\alpha\theta}{2\sin\theta}d\theta$$

$$I_{27} = \int_0^{\theta} \frac{-6.9389\times10^{-18}\theta}{2\sin\theta}d\theta$$

$$I_{28} = \int_0^{\theta} \frac{0.2556\sqrt{\theta}\alpha}{2\sin\theta}d\theta$$

$$I_{29} = \int_0^{\theta} \frac{-0.6176R\sqrt{\theta}}{2P_r\sin\theta}d\theta$$

$$I_{30} = \int_0^{\theta} \frac{1.8498\times10^{-17}\sqrt{\theta}\ln\theta}{2P_r\sin\theta}d\theta$$

$$I_{31} = \int_0^{\theta} \frac{-2.0586\sqrt{\theta}}{2P_r\sin\theta}d\theta$$

$$I_{32} = \int_0^{\theta} \frac{0.3114\sqrt{\theta}}{2\sin\theta}d\theta$$

$$I_{33} = \int_0^{\theta} \frac{3.4696\times10^{-18}\alpha(\theta-\sin\theta\cos\theta)}{2\sin\theta}d\theta$$

$$I_{34} = \int_0^{\theta} \frac{0.97091R(\theta-\sin\theta\cos\theta)}{2P_r\sin\theta\sqrt{\theta}}d\theta$$

$$I_{35} = \int_0^{\theta} \frac{-1.1654\times10^{-17}(\theta-\sin\theta\cos\theta)}{2\sin\theta\sqrt{\theta}}d\theta$$

$$I_{36} = \int_0^{6} \frac{0.32337(\theta-\sin\theta\cos\theta)}{2P_r\sin\theta\sqrt{\theta}}d\theta$$

$$I_{37} = \int_0^{\theta} \frac{0.7875(\theta-\sin\theta\cos\theta)}{2\sin\theta\sqrt{\theta}}d\theta$$

$$I_{38} = \frac{-3.0791\times10^{-18}\alpha(\theta-\sin\theta\cos\theta)}{2\sin\theta\theta^{\frac{3}{2}}}d\theta$$

$$I_{39} = \int_0^{\theta} \frac{2.8112\times10^{-19}(\theta-\sin\theta\cos\theta)}{2\sin\theta\theta^{\frac{3}{2}}}d\theta$$

$$I_{40} = \int_0^{\theta} \frac{-8.6736\times10^{-18}(\theta-\sin\theta\cos\theta)}{2\sin\theta}d\theta$$

$$I_{41} = \int_0^{\theta} \frac{6.9389\times10^{-18}\cos^2\theta}{2\sin\theta}d\theta$$

Appendix B. Non-integrable functions in series form

$$I_1 \approxeq \sqrt{\theta}\big(-0.02 - 2.24346\times10^{-18}\theta + 0.012\theta^2 - 1.66533 + 10^{-18}\theta^3 - 0.006666667\theta^4\big) + \cdots$$

$$I_2 \approxeq \sqrt{\theta}\big(0.02 - 0.008\theta^2 + 0.00148148\theta^4\big) + \cdots$$

$$I_3 \approxeq \theta^{\frac{3}{2}}\big(-0.0066666 + 0.00571429\theta^2 - 0.0066666\theta^{\frac{9}{2}}\big) + \cdots$$

$$I_4 \approxeq \theta^{\frac{3}{2}}\big(0.00666667 - 1.25673\times10^{3}\theta^2 - 1.09176\times10^{-18}\theta^3 + 0.00387879\theta^4\big) + \cdots$$

$$I_5 \approxeq \theta^{\frac{3}{2}}\big(-0.006667 + 6.48634\times10^{-19}\theta + 0.00190476\theta^2 + 1.31582\times10^{-19}\theta^3 - 0.0002424\theta^4\big) + \cdots$$

$$I_6 \approxeq \theta + \frac{\theta^3}{6} + \frac{7\theta^5}{360} + \cdots,\ I_7 \approxeq \frac{\theta^2}{2} + \frac{\theta^4}{24} + \frac{7\theta^6}{2160} + \cdots,$$

$$I_8 \approxeq \frac{0.97091R}{P_r\sqrt{\theta}} + \frac{0.26967R\theta^{\frac{3}{2}}}{Pr} + \cdots$$

$$I_9 \approxeq \frac{-1.1654\times10^{-17}}{\sqrt{\theta}} - 3.23722\times10^{-18}\theta^{\frac{3}{2}} + \cdots$$

$$I_{10} \approxeq \frac{0.32337}{P_r\sqrt{\theta}} + \frac{0.089825\theta^{\frac{3}{2}}}{P_r} + \cdots$$

$$I_{11} \approxeq \frac{0.7875}{\sqrt{\theta}} + 0.21875\theta^{\frac{3}{2}} + \cdots\ I_{12} \approxeq \frac{-1.02637\times10^{-18}\alpha}{\theta^{\frac{3}{2}}} - \frac{1.56482\times10^{-33}\theta}{\theta^{\frac{3}{2}}} - \frac{2.56592\times10^{-18}\theta^2\alpha}{\theta^{\frac{3}{2}}} + \frac{6.561\times10^{-35}\theta^3\alpha}{\theta^{\frac{3}{2}}} + \frac{1.14611\times10^{-19}\theta^4\alpha}{\theta^{\frac{3}{2}}} + \cdots$$

$$I_{13} \approxeq \frac{9.3707\times10^{-20}}{\theta^{\frac{3}{2}}} + \frac{1.5423\times10^{-34}\theta}{\theta^{\frac{3}{2}}} + \frac{2.3427\times10^{-19}\theta^2}{\theta^{\frac{3}{2}}}$$

$$-\frac{7.5028\times10^{-36}\theta^3}{\theta^{\frac{3}{2}}}$$

$$+\frac{1.0464\times10^{-20}\theta^4}{\theta^{\frac{3}{2}}}+\cdots\quad I_{14}\approxeq-1.1223\times10^{-34}\alpha\theta$$

$$+3.1175\times10^{-35}\alpha\theta^3+\cdots,$$

$$I_{15}\approxeq-0.2556\alpha\sqrt{\theta}+0.0426\theta^{\frac{5}{2}}+\cdots$$

$$I_{16}\approxeq\frac{0.6176R\sqrt{\theta}}{P_r}-\frac{0.102933R\theta^{\frac{5}{2}}}{P_r}+\cdots$$

$$I_{17}\approxeq3.6996\times10^{-17}\sqrt{\theta}-1.2332\times10^{-18}\theta^{\frac{5}{2}}-1.8498\times10^{-17}\sqrt{\theta}\ln\theta$$

$$+3.083\times10^{-18}\theta^{\frac{5}{2}}\ln\theta+\cdots\quad I_{18}\approxeq\frac{2.0586\sqrt{\theta}}{P_r}-\frac{0.3431\theta^{\frac{5}{2}}}{P_r}+\cdots$$

$$I_{19}\approxeq-0.3114\sqrt{\theta}+0.0519\theta^{\frac{5}{2}}+\cdots$$

$$I_{20}\approxeq-\frac{0.97091R}{P_r\sqrt{\theta}}+\frac{0.0539394R\theta^{\frac{3}{2}}}{P_r}+\cdots$$

$$I_{21}\approxeq\frac{1.1654\times10^{-17}}{\sqrt{\theta}}-6.7444\times10^{-19}\theta^{\frac{3}{2}}+\cdots$$

$$I_{22}\approxeq\frac{-0.32337}{P_r\sqrt{\theta}}+\frac{0.089825\theta^{\frac{3}{2}}}{P_r}+\cdots$$

$$I_{23}\approxeq\frac{-0.7875}{\sqrt{\theta}}+0.21875\theta^{\frac{3}{2}}+\cdots$$

$$I_{24}\approxeq\frac{1.02637\times10^{-18}\alpha}{\theta^{\frac{3}{2}}}-\frac{5.77779\times10^{-34}\alpha\theta}{\theta^{\frac{3}{2}}}$$

$$-\frac{5.13183\times10^{-19}\alpha\theta^2}{\theta^{\frac{3}{2}}}+\frac{1.77255\times10^{-35}\alpha\theta^3}{\theta^{\frac{3}{2}}}-\frac{1.19743\times10^{-20}\alpha\theta^4}{\theta^{\frac{3}{2}}}+\cdots$$

$$I_{25}\approxeq\frac{9.37067\times10^{-20}}{\theta^{\frac{3}{2}}}+\frac{9.62965\times10^{-35}\theta}{\theta^{\frac{3}{2}}}+\frac{4.68533\times10^{-20}\theta^2}{\theta^{\frac{3}{2}}}$$

$$-\frac{1.61833\times10^{-36}\theta^3}{\theta^{\frac{3}{2}}}+\frac{1.09324\times10^{-21}\theta^4}{\theta^{\frac{3}{2}}}+\cdots$$

$$I_{26}\approxeq1.223\times10^{-34}\alpha\theta+6.235\times10^{-36}\alpha\theta^3+\cdots$$

$$I_{27}\approxeq-3.46945\times10^{-18}-1.92747\times10^{-19}\theta^3+\cdots$$

$$I_{28}\approxeq0.2556\alpha\sqrt{\theta}+0.00852\alpha\theta^{\frac{5}{2}}+\cdots$$

$$I_{29}\approxeq\frac{-0.6176R\sqrt{\theta}}{P_r}-\frac{0.0205867R\theta^{\frac{5}{2}}}{P_r}+\cdots$$

$$I_{30}\approxeq-3.6996\times10^{-17}\sqrt{\theta}-2.4664\times10^{-19}\theta^{\frac{5}{2}}+1.8498\times10^{-17}\sqrt{\theta}\ln\theta$$

$$+6.166\times10^{-19}\theta^{\frac{5}{2}}\ln\theta+\cdots$$

$$I_{31}\approxeq\frac{-2.0586\sqrt{\theta}}{P_r}-\frac{0.06862\theta^{\frac{5}{2}}}{P_r}+\cdots\quad I_{32}\approxeq0.3114\sqrt{\theta}+0.01038\theta^{\frac{5}{2}}+\cdots$$

$$I_{33}\approxeq3.85511\times10^{-19}\theta^3\alpha+\cdots\quad I_{34}\approxeq\frac{0.129455R\theta^{\frac{5}{2}}}{P_r}+\cdots$$

$$I_{35}\approxeq-1.55387\times10^{-18}\theta^{\frac{5}{2}}+\cdots\quad I_{36}\approxeq-1.55387\times10^{-18}\theta^{\frac{5}{2}}+\cdots$$

$$I_{37}\approxeq\frac{0.043116\theta^{\frac{5}{2}}}{P_r}+\cdots$$

$$I_{38}\approxeq0.105\theta^{\frac{5}{2}}+\cdots\quad I_{39}\approxeq-6.84244\times10^{-19}\theta^{\frac{3}{2}}\alpha+\cdots$$

$$I_{40}\approxeq6.24711\times10^{-20}\theta^{\frac{3}{2}}+\cdots$$

$$I_{41}\approxeq-9.63733\times10^{-19}\theta^3+\cdots$$

Appendix C. Integration constant

$$a_1=0.0137593$$

$$a_2=\frac{-0.118586}{1.9687}$$

$$a_3=0.$$

$$b_1=\alpha+3+\frac{\pi}{2}+\frac{\pi^3}{144}+\frac{7\pi^5}{57600}$$

$$b_2=\frac{-16\pi\left(43200+1800\pi^2+\frac{45\pi^4}{2}+\frac{7\pi^6}{45}\right)}{86400\pi^2}$$

$$+\frac{172800\alpha\pi}{86400\pi^2}-\frac{144\pi\alpha\left(1800+25\pi^2+\frac{7\pi^4}{16}\right)}{86400\pi^2}$$

$$b_3=3$$

$$j_1=0.18861\alpha-0.829203-\frac{1}{P_r}\left[1.95391+1.76136R\right]$$

$$j_2=-0.63662\left[-0.205958+0.43689\alpha-1\times10^{-21}\left(2.98817\times10^{12}\alpha+\right.\right.$$

$$\left.\left.\frac{1.02259\times10^{10}}{P_r}+\frac{3.07029\times10^{10}R}{P_r}\right)-\frac{3.82184}{P_r}-\frac{1.9658}{P_r}\right]$$

$$j_3=0$$

References

[1] F.E. Culick, Acoustic oscillations in solid propellant rocket chambers, Astronaut. Acta 12 (2) (1966) 113–126.
[2] F.E.C. Culick, Rotational axisymmetric mean flow and damping of acoustic waves in asolid propellant rocket, AIAA J. 4 (8) (1966) 1462–1464.
[3] G.A. Flandro, J. Majdalani, Aeroacoustic instability in rockets, AIAA J. 41 (3) (2003) 485–497.
[4] F.E.C. Culick, Stability of longitudinal oscillations with pressure and velocity coupling in a solid propellant rocket, Combust. Sci. Technol. 2 (4) (1970) 179–201.
[5] J. Majdalani, On steady rotational high speed flows: the compressible Taylor–Culick profile, Proc. R. Soc. Lond. Ser. A Math. Phys. Eng. Sci. 463 (2077) (2007) 131–162.
[6] A.S. Berman, Laminar flow in channels with porous walls, J. Appl. Phys. 24 (9) (1953) 1232–1235.
[7] R.M. Terrill, P.W. Thomas, On laminar flow through a uniformly porous pipe, Appl. Sci. Res. 21 (1) (1969) 37–67.
[8] S. Chellm, M. Liu, Effect of slip on existence, uniqueness and behaviour of similarity solutions for steady incompressible laminar flow in porous tubes and channels, Phys. Fluids 18 (2006) 083601–083610.
[9] J.F. Brady, Flow development in a porous channel and tube, Phys. Fluids 27 (5) (1984) 1061–1067.
[10] J.P. Quaile, E.K. Levy, Laminar flow in a porous tube with suction, 1975.
[11] L.S. Galowin, M.J. Desantis, Theoretical analysis of laminar pipe flow in a porous wall cylinder, 1971.
[12] T. Saad, J. Majdalani, Viscous mean flow approximations for porous tubes with radially regressing walls, AIAA J. 55 (11) (2017) 3868–3880.
[13] C. Zhou, J. Majdalani, Improved mean-flow solution for slab rocket motors with regressing walls, J. Propul. Power 18 (3) (2002) 703–711.
[14] Y.Z. Boutros, M.B. Abd-el Malek, N.A. Badran, H.S. Hassan, Lie-group method for unsteady flows in a semi-infinite expanding or contracting pipe with injection or suction through a porous wall, J. Comput. Appl. Math. 197 (2) (2006) 465–494.
[15] B.E. Pearce, Radiative heat transfer within a solid-propellant rocket motor, J. Spacecr. Rockets 15 (2) (1978) 125–128.
[16] X.L. Xia, D.P. Ren, H.P. Tan, Thermal radiation effects of a high-temperature developing laminar flow in a tube, Heat Transfer—Asian Res.: Co-Sponsored Soc. Chem. Eng. Japan Heat Transfer Div. ASME 33 (5) (2004) 299–306.
[17] R. Viskanta, Interaction of heat transfer by conduction, convection, and radiation in a radiating fluid, 1963.
[18] J.M. Huang, J.D. Lin, Combined radiative and forced onvective heat transfer in hermally-developing laminar flow hrough a circular pipe, Chem. Eng. Commun. 101 (1) (1991) 147–164.
[19] V. Hariprasad, P. Sankar, P. Shivahari, V.R. Kumar, Studies on gravity influence on solid propellant burn rate, in: Applied Mechanics and Materials, Vol. 232, Trans Tech Publications Ltd, 2012, pp. 342–347.
[20] H. Ishigaki, The effect of buoyancy on laminar flow and heat transfer in pipes, JSME Int. J. Ser. B Fluids Therm. Eng. 40 (2) (1997) 273–280.
[21] C. Griego, N. Yilmaz, A. Atmanli, Analysis of aluminum particle combustion in a downward burning solid rocket propellant, Fuel 237 (2019) 405–412.
[22] C. Griego, N. Yilmaz, A. Atmanli, Sensitivity analysis and uncertainty quantification on aluminum particle combustion for an upward burning solid rocket propellant, Fuel 237 (2019) 1177–1185.
[23] L.V.E. Ovsiannikov, Group Analysis of Differential Equations, Academic Press, 2014.
[24] P.J. Olver, Applications of Lie Groups to Differential Equations, Vol. 107, Springer Science and Business Media, 2000.
[25] G.W. Bluman, S. Kumei, Symmetries and Differential Equations, Vol. 81, Springer Science and Business Media, 2013.
[26] N.H. Ibragimov, Transformation Groups Applied to Mathematical Physics, Vol. 3, Springer Science and Business Media, 1984.

[27] N.H. Ibragimov, CRC Handbook of Lie Group Analysis of Differential Equations, Vol. 3, CRC Press, 1995.
[28] M. Azimi, A.M. Hedesh, S. Karimian, Flow modeling in a porous cylinder with regressing walls using semi analytical approach, Mech. Mech. Eng. 18 (2) (2014) 77–84.
[29] R. Kandasamy, I. Muhaimin, N.S. Amin, Lie group analysis for the effect of temperature-dependent fluid viscosity with thermophoresis on magnetohydrodynamic free convective heat and mass transfer over a porous stretching surface, Int. J. Comput. Fluid Dyn. 24 (1–2) (2010) 1–11.
[30] W.W. Chu, V. Yang, J. Majdalani, Premixed flame response to acoustic waves in a porous-walled chamber with surface mass injection, Combust. Flame 133 (3) (2003) 359–370.
[31] A.B. Vyas, J. Majdalani, V. Yang, Estimation of the laminar premixed flame temperature and velocity in injection-driven combustion chambers, Combust. Flame 133 (3) (2003) 371–374.
[32] J. Song, W. An, Y. Wu, W. Tian, Neutronics and thermal hydraulics analysis of a conceptual ultra-high temperature MHD cermet fuel core for nuclear electric propulsion, Front. Energy Res. 6 (2018) 29.